POLITECNICO DI TORINO
Repository ISTITUZIONALE

Designing the mechanical behavior of NiTi self-expandable vascular stents by tuning the heat treatment parameters

Original
Designing the mechanical behavior of NiTi self-expandable vascular stents by tuning the heat treatment parameters / Carbonaro, Dario; Villa, Elena; Gallo, Diego; Morbiducci, Umberto; Audenino, Alberto; Chiastra, Claudio. - In: JOURNAL OF THE MECHANICAL BEHAVIOR OF BIOMEDICAL MATERIALS. - ISSN 1751-6161. - ELETTRONICO. - 158:(2024), pp. 1-11. [10.1016/j.jmbbm.2024.106653]

Availability:
This version is available at: 11583/2999361 since: 2025-04-18T13:22:06Z

Publisher:
Elsevier

Published
DOI:10.1016/j.jmbbm.2024.106653

Terms of use:

This article is made available under terms and conditions as specified in the corresponding bibliographic description in the repository

Publisher copyright

(Article begins on next page)

07 May 2026

journal of the mechanical behavior of biomedical materials 158 (2024) 106653

Contents lists available at ScienceDirect

Journal of the Mechanical Behavior of Biomedical Materials

journal homepage: www.elsevier.com/locate/jmbbm

Designing the mechanical behavior of NiTi self-expandable vascular stents by tuning the heat treatment parameters

Dario Carbonaro [a], Elena Villa [b], Diego Gallo [a], Umberto Morbiducci [a], Alberto Luigi Audenino [a,*], Claudio Chiastra [a]

[a] PoliTo^{BIO}Med Lab, Department of Mechanical and Aerospace Engineering, Politecnico di Torino, Turin, Italy
[b] National Research Council, Institute of Condensed Matter Chemistry and Technologies for Energy (CNR-ICMATE), Lecco, Italy

ARTICLE INFO

Keywords:
Nitinol
Shape memory alloy
Material processing
Stent-graft
Computational modelling
Finite element analysis

ABSTRACT

The remarkable mechanical properties of nickel-titanium (NiTi) shape memory alloy, particularly its super-elasticity, establish it as the material of choice for fabricating self-expanding vascular stents, including the metallic backbone of peripheral stents and the metallic frame of stent-grafts. The super-elastic nature of NiTi substantially influences the mechanical performance of vascular stents, thereby affecting their clinical effectiveness and safety. This property shows marked sensitivity to the primary parameters of the heat treatment process used in device fabrication, specifically temperature and processing time. In this context, this study integrates experimental and computational analyses to explore the potential of designing the mechanical characteristics of NiTi vascular stents by adjusting heat treatment parameters. To reach this aim, differently heat-treated NiTi wire samples were experimentally characterized using calorimetric and uniaxial tensile testing. Subsequently, the mechanical response of a stent-graft model featuring a metallic frame made of NiTi wire was assessed in terms of radial forces generated at various implantation diameters through finite element analysis. The stent-graft served as an illustrative case of NiTi vascular stent to investigate the impact of the heat treatment parameters on its mechanical response. From the study a strong linear relationship emerged between NiTi super-elastic parameters (i.e., austenite finish temperature, martensite elastic modulus, upper plateau stress, lower plateau stress and transformation strain) and heat treatment parameters ($R^2 > 0.79$, p-value < 0.001) for the adopted ranges of temperature and processing time. Additionally, a strong linear relationship was observed between: (i) the radial force generated by the stent-graft during expansion and the heat treatment parameters ($R^2 > 0.82$, p-value < 0.001); (ii) the radial force generated by the stent-graft during expansion and the lower plateau stress of NiTi ($R^2 > 0.93$, p-value < 0.001). In conclusion, the findings of this study suggest that designing and optimizing the mechanical properties of NiTi vascular stents by finely tuning temperature and processing time of the heat treatment process is feasible.

1. Introduction

Near-equiatomic nickel-titanium (NiTi), also known as Nitinol, is recognized for its distinctive super-elasticity and shape memory properties (Duerig et al., 1990). These unique properties have promoted the extensive utilization of NiTi in the field of medical devices (Kapoor, 2017; Pelton et al., 2000). In terms of super-elasticity, NiTi exhibits the capability to elastically recover large (up to 15 %) deformations (Auricchio et al., 1997). This property is associated with the capability to undergo a reversible transformation between two distinct solid phases in the NiTi lattice structure, known as austenite and martensite. At temperatures above the austenite finish temperature (A_f) (ASTM, 2015), typically below the body temperature for NiTi in medical applications (Duerig et al., 2003; Henderson et al., 2011), austenite is stable at low strain values, while martensite is stable at high strain values (Otsuka and Ren, 2005). Consequently, as a result of stress-induced conversion from austenite to martensite, the NiTi stress *vs.* strain curve is characterized by elastic hysteresis, with two plateaus in the loading and unloading phases where high strains are generated and recovered, respectively (Auricchio and Taylor, 1997).

Due to its super-elasticity, NiTi has established itself as the material of election for self-expanding vascular stents – medical implants

* Corresponding author.
E-mail address: alberto.audenino@polito.it (A.L. Audenino).

https://doi.org/10.1016/j.jmbbm.2024.106653
Received 23 April 2024; Received in revised form 14 June 2024; Accepted 6 July 2024
Available online 6 July 2024
1751-6161/© 2024 The Authors. Published by Elsevier Ltd. This is an open access article under the CC BY license (http://creativecommons.org/licenses/by/4.0/).

designed to automatically expand and conform to the shape and size of the patient's blood vessels without the need for any expansion support (Fanning et al., 2013; Pan et al., 2021). In detail, NiTi is used for the creation of the metallic backbone of peripheral stents and of the metallic frame of stent-grafts, enabling those devices to withstand and elastically recover considerable strains upon insertion into the catheter before being deployed (Stoeckel et al., 2004).

The super-elastic properties of NiTi have a substantial influence on the mechanical performance of the devices, and consequently, on their clinical effectiveness and safety (Cabrera et al., 2017; Carbonaro et al., 2024, 2023d). Experimental findings have highlighted considerable variability in the super-elastic properties of NiTi, depending on the chemical composition, grain size and distribution, as well as the processing methods and the history of the material (Hodgson and Russell, 2000; Kapoor, 2017; Liu and Mishnaevsky, 2013; Mwangi et al., 2019; Pelton et al., 2000; Valiev et al., 2020). Specifically, shape-setting constitutes a crucial processing step of a NiTi vascular stent, involving securing the device in a fixture in the desired configuration and subjecting it to heat treatment (Bernini et al., 2024; Hodgson and Russell, 2000). Previous experimental investigations on NiTi samples highlighted a marked sensitivity of NiTi A_f and nonlinear stress *vs.* stress curve to operating temperature and processing time of the applied heat treatment (Agarwal et al., 2023; Liu et al., 2008; Zhan et al., 2020). However, the relationship between heat treatment parameters and the material properties of NiTi, and consequently the mechanical performance of NiTi vascular stents, is often proprietary knowledge of the material suppliers and medical device companies and is not adequately documented in the current literature. This paucity of documentation available to all markedly limits research and product innovation of NiTi medical devices.

In this context, the present study explores the potential of designing the mechanical characteristics of NiTi vascular stents by adjusting heat treatment parameters, specifically temperature and processing time. In detail, the relationship between the heat treatment parameters and the material properties of NiTi was experimentally determined through calorimetric analysis and uniaxial tensile testing on wire samples. Next, the impact of the heat treatment parameters on the mechanical behavior of an illustrative stent-graft model, featuring a metallic frame made of NiTi wires with the same cross-section as the wire samples, was assessed through finite element (FE) analysis. Lasty, the relationship between the material properties of NiTi at various combinations of heat treatment parameters and the mechanical behavior of the stent-graft was examined to better elucidate how the heat treatment process can impact the mechanical behavior of the device.

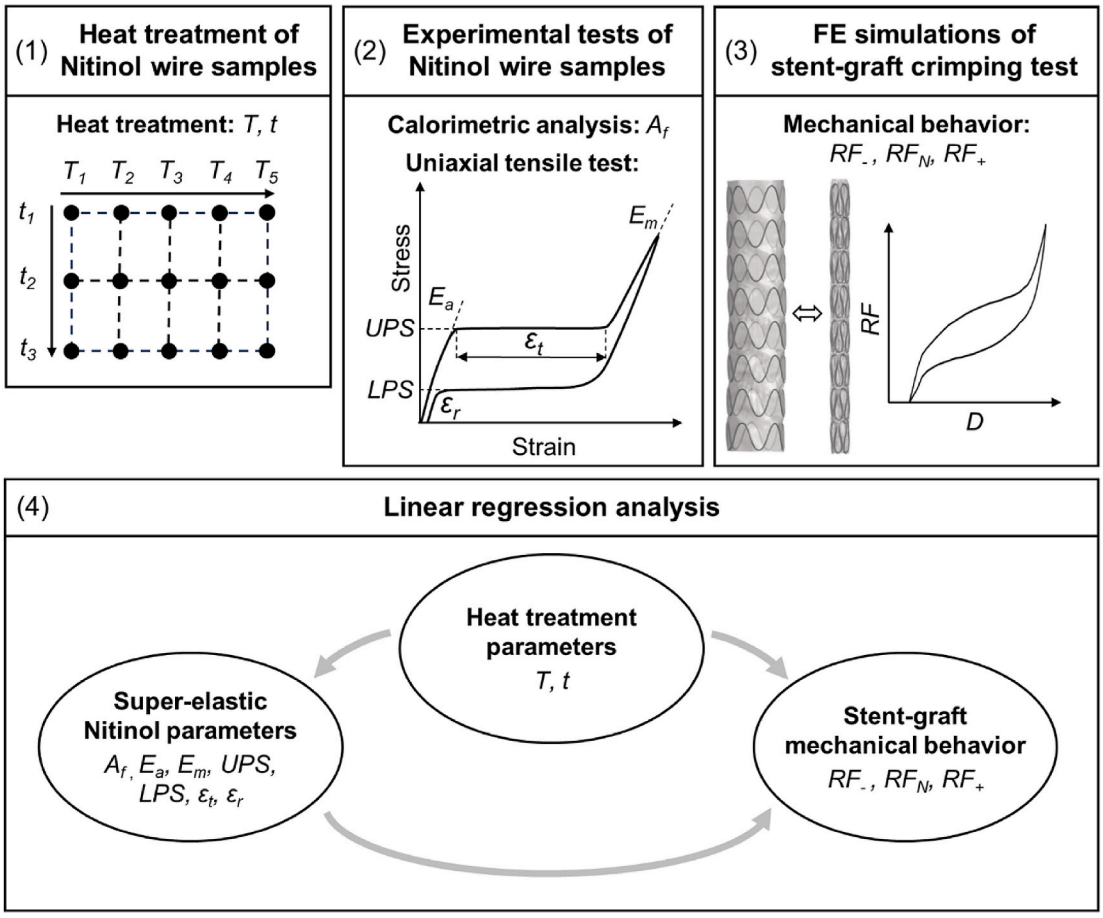

Fig. 1. Main steps of the procedure employed in this study: Step 1 – Heat treatment of NiTi wire samples, based on fifteen combinations of temperature (T) and processing time (t) values, considering five T values (i.e., T_1, T_2, T_3, T_4 and T_5) and three t values (i.e., t_1, t_2, and t_3); Step 2 – Experimental testing of NiTi wire samples, including calorimetric analysis, measuring the austenite finish temperature (A_f), and uniaxial tensile testing, measuring the austenite elastic modulus (E_a), martensite elastic modulus (E_m), upper plateau stress (*UPS*), lower plateau stress (*LPS*), transformation strain (ε_t) and residual strain (ε_r); Step 3 – FE simulation of the crimping test of a stent-graft with a frame made of NiTi wire rings, evaluating the radial force (*RF*) at three distinct implantation diameters (D) (i.e., RF_-, RF_N and RF_+). Step 4 - Following step 2, (i) the relationship between T and t with the material parameters derived from the calorimetric analyses and uniaxial tensile tests (i.e., A_f, E_a, E_m, *UPS*, *LPS*, ε_t and ε_r); Following step 3, (ii) the relationship between T and t and the parameters obtained from FE simulations of crimping test of the stent-graft (i.e., RF_-, RF_N, and RF_+); Following step 3, the relationship between some of the material parameters (i.e., E_a, E_m, *UPS*, *LPS*, ε_t) and RF_-, RF_N, and RF_+.

2. Methods

The procedure employed in this study is based on the following main steps (Fig. 1): Step 1 – Heat treatment of NiTi wire samples, considering different temperature (T) and processing time (t) settings; Step 2 – Experimental characterization of NiTi wire samples, involving calorimetric analysis and uniaxial tensile testing; Step 3 – FE simulations of crimping tests on stent-grafts made of differently heat-treated NiTi wires to evaluate their mechanical response in terms of radial force (*RF*) *vs.* diameter (*D*); Step 4 – Statistical analysis to investigate the existence of possible links among heat treatment parameters, NiTi material parameters, and the mechanical behavior of the stent-graft.

2.1. Heat treatment of NiTi wire samples

Fifteen samples (identified as sample 1 to 15) of straight annealed NiTi wire, certified as biomedical grade according to ASTM F2063-18 (ASTM, 2018) (Ni content between 54.5 % and 57.0 % in weight percentage), were provided by Admedes (Admedes GmbH, Pforzheim, Germany). The NiTi wire samples had a diameter of 0.6 mm and were cut to a length of 100 mm. Each wire sample underwent heat treatment with a specific combination of processing temperature T and time t (Fig. 1, Step 1), utilizing the fluidized sand bath Techne FB-08C (Bibby Scientific, Stone, United Kingdom). In total, fifteen combinations of heat treatment parameters were tested, considering five T values (T_1 = 485 °C, T_2 = 500 °C, T_3 = 515 °C, T_4 = 530 °C and T_5 = 545 °C) and three t values (t_1 = 150 s, t_2 = 300 s and t_3 = 450 s). The ranges of T and t were based on values commonly adopted by stent manufacturers for heat treatment.

2.2. Experimental testing of NiTi wire samples

2.2.1. Calorimetric analysis

Differential scanning calorimetry (DSC) analyses were performed on NiTi wire samples after their heat treatment to determine their austenite finish temperature (A_f) (ASTM, 2015). The DSC 25 calorimeter equipped by an RCS cooling system (TA Instruments, New Castle, DE, USA) was utilized for this purpose. DSC curves were acquired within the temperature range of [−90 °C, 120 °C] and with a rate of 10 °C/min.

2.2.2. Uniaxial tensile testing

Uniaxial tensile tests were conducted on the fifteen NiTi wire samples post heat treatment using the E3000 tensile testing machine equipped with a thermal chamber and an integrated optical extensometer (Instron, Norwood, MA, USA). A 3 kN load cell and flat grips were utilized for the tests (Henderson et al., 2011). The experiments were conducted at a strain rate of 2 %/min and at 37 °C to replicate body temperature, which serves as the reference temperature for testing NiTi vascular stents (FDA, 2010; ISO, 2012). The uniaxial testing procedure comprised an initial pre-conditioning cycle, followed by four subsequent cycles, each one reaching a strain level of 9 %, and concluded by a final cycle extended until the fracture of the samples was obtained. Accordingly, the stress *vs.* strain curve was measured. For each curve, the following material parameters characterizing the super-elastic properties of NiTi were determined from the first cycle after pre-conditioning (Step 2 in Fig. 1): austenite elastic modulus (E_a), martensite elastic modulus (E_m), upper plateau stress (*UPS*), lower plateau stress (*LPS*), transformation strain (ε_t), and residual strain after the first cycle (ε_r). Moreover, the ultimate tensile strength (*UTS*) was measured in the break cycle. *UPS* and *LPS* values were computed from the stress *vs.* strain curves as the average stress values of the straight part of the plateaus, which were identified by changes in the derivative of the curve.

2.3. FE simulations of stent-graft crimping test

2.3.1. FE model of the stent-graft

The FE model of a self-expandable thoracic aortic stent-graft was constructed using Hypermesh (Altair Engineering, Troy, MI, USA) in conjunction with Abaqus/Explicit (Dassault Systemes Simulia Corp., Johnston, RI, USA). A geometry inspired by the commercially available Valiant™ stent-graft (Medtronic, Dublin, Ireland) was created, featuring a diameter of 30 mm and a length of 150 mm (Step 3 in Fig. 1). The device was assumed to be composed of eight stent rings made of NiTi wires with a diameter of 0.6 mm (consistent with the NiTi wire samples), sutured to a polytetrafluoroethylene (ePTFE) graft with a thickness of 0.1 mm. In the FE models, the graft was included along with the NiTi rings to ensure an accurate mechanical representation of the device. The stent rings were meshed with B31 two-node linear beam elements with an average size of 1 mm (Ramella et al., 2022). The graft was meshed with S3 three-node linear shell elements, having an average size of 1 mm (Ramella et al., 2022). The mechanical behavior of NiTi was described using the super-elastic constitutive model by Auricchio and Taylor (1997), with the super-elastic material parameters of each NiTi wire sample introduced in section 2.2.2 integrated into the constitutive model. In this model (Fig. 1), material asymmetry between traction and compression loading is accounted for by one model parameter. Due to challenges in testing thin NiTi wire samples in compression (Henderson et al., 2011), a ratio of 1.5 between the *UPS* in compression and traction loading was here assumed, according to previous studies (Carbonaro et al., 2023d; Kan et al., 2021). Additionally, Poisson ratios for austenite and martensite phases were considered equal to 0.3 (Carbonaro et al., 2023d). Finally, the ε_r and *UTS* were not included, as they are not considered in the super-elastic constitutive model (Auricchio and Taylor, 1997). The mechanical behavior of ePTFE was described with an elasto-plastic constitutive model with material properties obtained from previous studies (E = 55.2 MPa, σ_{yield} = 6.6 MPa) (Catanese et al., 1999; Kleinstreuer et al., 2008).

The FE model of the stent-graft was created by assembling the stent rings with the graft. Since the stent-graft is characterized by stent prestress in the sutured configuration, this condition was taken into account in the FE model following the procedure suggested by Ramella et al. (2022) and illustrated in Fig. 2(a). In detail, a preliminary FE analysis was conducted using Abaqus/Explicit in which the NiTi rings were moved from the stress-free configuration to the graft by imposing radial displacement. Subsequently, tied contacts between the stent rings and the graft were activated to allow the device to assume its final configuration.

2.3.2. FE simulation of the crimping test

The radial crimping test is the standard procedure used to assess the mechanical behavior of vascular stents under radial displacement (FDA, 2010; ISO, 2012). In the case of stent-grafts, it aims to replicate the loading conditions experienced by these devices when they are inserted into a catheter and deployed into the aorta. The test allows for the measurement of the *RF* as a function of *D*, evaluating whether the stent-graft applies a sufficiently high *RF* to the aortic wall upon implantation to ensure proper fixation (Senf et al., 2014; Zarins et al., 2003).

Simulations of the radial crimping procedure were performed using the FE code Abaqus/Explicit on 6 computing cores of a workstation equipped with Intel® Core™ i7-8700 and 32 GB RAM. Fifteen FE simulations, each corresponding to a unique combination of material parameters associated with the NiTi wire samples, were performed. The radial crimping of the stent was simulated through contact with a crimping cylinder modelled as rigid material and discretized using SFM3D4R four-node elements (Kan et al., 2021). The simulated crimping cylinder, which replicated the testing machine typically employed in experimental radial crimping tests (Cabrera et al., 2017), was radially compressed, without any nodes of the stent-graft being constrained.

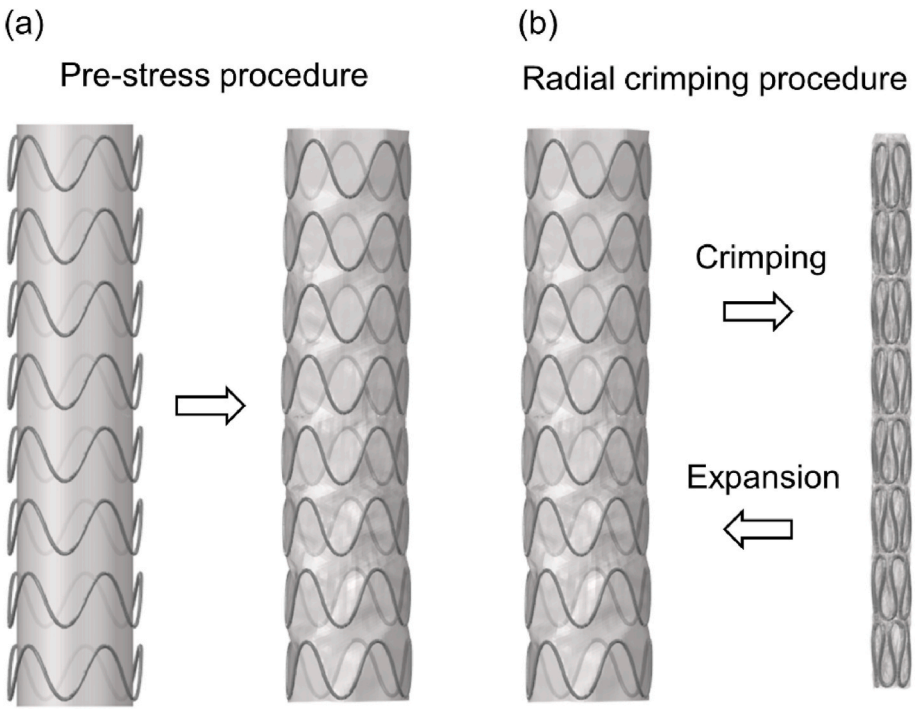

Fig. 2. (a) Pre-stress procedure of the stent-graft in the sutured configuration; (b) Radial crimping procedure, which comprises the crimping step followed by the expansion step.

Before simulating the radial crimping procedure, a uniform temperature field of 37 °C was applied to all nodes of the model. Technically, the radial crimping procedure was simulated in two steps, namely the crimping and expansion steps (Fig. 2(b)). In the crimping step, the stent-graft was crimped starting from its initial D to a minimum D of 10 mm. In the expansion step, the stent-graft was released, returning to its initial D. Interactions between stent-graft and crimping cylinder were modelled applying a general contact algorithm where the default "hard" normal contact behavior was employed, with tangential behavior defined using friction coefficient values $\mu = 0.3$ and $\mu = 0.1$ for the stent rings/crimping cylinder interaction and self-contact between the stent rings, and for the graft/crimping cylinder interaction, respectively (Ramella et al., 2022). Furthermore, to ensure a quasi-static analysis, it was verified that the ratio of kinetic energy to total internal strain energy was less than 5 % (Carbonaro et al., 2023b).

The RF was computed at different D values, selected to be representative of aortic dimensions where the device is typically implanted. In detail, RF was quantified in terms of RF_N, RF_- and RF_+ values, calculated during the simulated expansion step at $D_N = 25$ mm, $D_- = 23$ mm and $D_+ = 27$ mm, respectively. The rationale for this choice lies in the fact that these diameters correspond to the nominal, minimum, and maximum recommended implantation diameters for the considered stent-graft size, as specified by the device manufacturer. The RF was computed as the sum of the generated contact normal forces between the stent-graft and the crimping cylinder along the radial direction (Step 3 in Fig. 1) (Carbonaro et al., 2020, 2023c).

2.4. Multivariate regression analysis

Multivariate linear regression analysis was conducted in Matlab (MathWorks, Natick, MA, USA) environment to investigate the existence of three distinct relationships, as schematized in Fig. 1: (i) following step 2, the relationship between heat treatment parameters (T and t) and the NiTi material parameters derived from calorimetric analysis and uniaxial tensile tests (A_f, E_a, E_m, UPS, LPS, ε_t, ε_r); (ii) following step 3, the relationship between heat treatment parameters (T and t) and the results obtained from the FE simulations of the stent-graft crimping test in terms of RF at different D values (RF_-, RF_N, and RF_+); and (iii) following step 3, the relationship between NiTi material parameters (E_a, E_m, UPS, LPS, ε_t) and the RF generated by the stent-graft at different D values (RF_-, RF_N, and RF_+). Strength and significance of the relationships was assessed in terms of coefficient of determination (R^2) and p-value of the F-test, respectively (Freund et al., 2010). Additionally, the unstandardized coefficients of the multivariate linear regression models were obtained, and for each coefficient, the corresponding p-value was determined. Preliminarily, the multivariate regression models were constructed considering all parameters. Then, in cases where coefficients had non-significant p-values, the corresponding parameters were removed from the model, and the remaining parameters were used to construct a new model. Statistical significance was assumed when p-values were lower than 0.05.

3. Results

3.1. Experimental tests of NiTi wire samples

3.1.1. Calorimetric analysis

Fig. 3 illustrates the DSC curve for NiTi wire sample 1, taken as a representative example. The A_f value for sample 1 was identified as 22.8 °C from the DSC curve. For completeness, the DSC curves of all NiTi wires samples by varying T and fixing t = 150 s, 300 s, 450 s, are included in the Supplementary material (Fig. S1). Table 1 reports the A_f values of all samples, which varied within the range [−3 °C, 23.8 °C]. These values were below the temperature of 37 °C, applied during the uniaxial tensile testing. As a result, all samples exhibited super-elastic behavior at 37 °C, meeting a fundamental requirement for the construction of implantable medical devices where this material behavior is essential (Duerig et al., 2003; Kapoor, 2017).

3.1.2. Uniaxial tensile tests

Fig. 4 depicts the uniaxial tensile stress *vs.* strain curve for NiTi wire sample 1, serving as a representative example. The figure includes

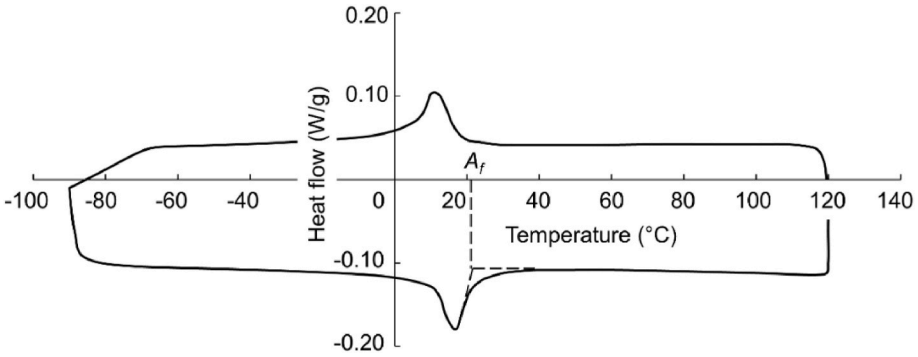

Fig. 3. DSC curve of NiTi wire sample 1, with representation of the austenite finish temperature (A_f).

Table 1
Results of the calorimetric and uniaxial tensile tests of the fifteen NiTi wire samples.

NiTi wire sample	T (°C)	t (s)	A_f (°C)	E_a (MPa)	E_m (MPa)	*UPS* (MPa)	*LPS* (MPa)	ε_t (%)	ε_r (%)	*UTS* (MPa)
1	485	150	22.8	60000	27400	515.9	192.1	4.8	0.38	1202.1
2	485	300	23.8	59100	26700	496.6	164.4	4.9	0.50	1133.7
3	485	450	23.7	59400	27200	479.2	132.8	4.7	0.52	1191.4
4	500	150	17.2	59700	28000	515.7	198.2	4.8	0.49	1204.5
5	500	300	19.6	61700	27100	499.9	173.6	5.0	0.58	1235.8
6	500	450	20.8	60050	26500	474.2	139.5	5.1	0.53	1196.8
7	515	150	14.8	61500	27500	528.2	209.4	5.1	0.38	1194.3
8	515	300	13.7	59500	26500	503.6	175.6	5.3	0.38	1130.8
9	515	450	14.6	59900	26000	484.6	169.1	5.2	0.64	1191.4
10	530	150	8.4	61150	26800	527.5	231.3	5.4	0.53	1133.7
11	530	300	6.2	60000	25700	509.9	188.0	5.6	0.56	1099.2
12	530	450	6.9	62100	26100	483.0	169.5	5.6	0.52	1070.0
13	545	150	−2.5	62300	26100	545.4	235.2	5.6	0.54	1053.0
14	545	300	−3.0	61400	25100	514.5	227.5	5.7	0.68	1147.0
15	545	450	−2.5	61500	25000	504.8	206.1	5.7	0.69	973.1
Minimum	485	150	−3.0	59100	25000	474.2	132.8	4.7	0.38	973.1
Maximum	545	450	23.8	62300	28000	545.4	231.3	5.7	0.69	1235.8

T: temperature; t: time; A_f: austenite finish temperature; E_a: austenite elastic modulus; E_m: martensite elastic modulus; *UPS*: upper plateau stress; *LPS*: lower plateau stress; ε_t: transformation strain; ε_r: residual strain; *UTS*: ultimate tensile strength.

representations of the four cycles of testing and the break cycle. Fig. 5 illustrates the uniaxial tensile stress *vs.* strain curves by varying T and fixing $t = 150$ s, and by varying t and fixing $T = 485$ °C, by considering only cycle 2. Uniaxial tensile stress *vs.* strain curves by varying T and fixing $t = 300$ s, 450 s, and by varying t and fixing $T = 500$ °C, 515 °C, 530 °C, 545 °C are included in the Supplementary material (Figs. S2 and S3). Table 1 reports the values of the material parameters for all the analyzed samples, which varied within the following ranges: $E_A \in$ [59100 MPa, 62300 MPa], $E_M \in$ [25000 MPa, 28000 MPa], *UPS* $\in$ [474.2 MPa, 545.4 MPa], *LPS* $\in$ [132.8 MPa, 231.3 MPa], $\varepsilon_t \in$ [4.7 %, 5.7 %], $\varepsilon_r \in$ [0.38 %, 0.69 %] and *UTS* $\in$ [973.1 MPa, 1235.8 MPa]. Fractures were observed at the extremes of the wire samples adjacent to the grips, suggesting that the measured *UTS* values may be conservative and uncertain. Accordingly, given this limitation, the *UTS* was excluded from the statistical analysis.

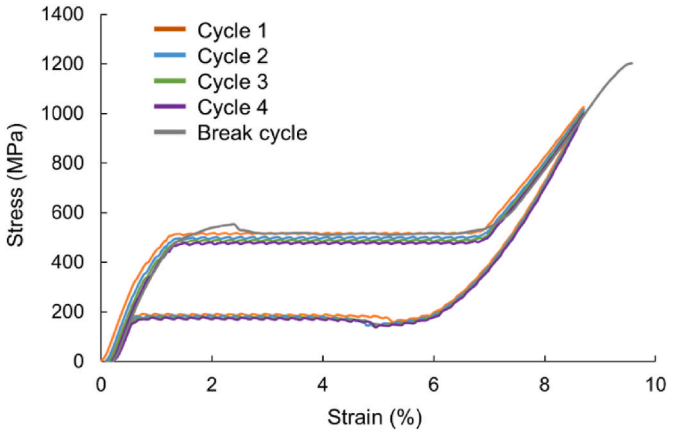

Fig. 4. Uniaxial tensile stress *vs.* strain curve of NiTi wire sample 1, including the four cycles of testing and the break cycle.

3.2. FE simulations of stent-graft crimping tests

Fig. 6 represents the *RF vs. D* curve obtained from the radial crimping test of the stent-graft, incorporating the material parameters of NiTi wire sample 1 (see Table 1). Typically, the *RF vs. D* curve exhibits a hysteresis cycle, a characteristic feature of self-expandable NiTi devices, including stent-grafts (Cabrera et al., 2017; Carbonaro et al., 2023c; Duerig et al., 2003; Ramella et al., 2022; Stoeckel et al., 2004). This mechanical behavior is characterized by higher radial forces during the crimping step compared to the expansion step, attributable to the super-elastic properties of NiTi. Additionally, Fig. 6 depicts the *RF* values RF_-, RF_N and RF_+, evaluated during the expansion step at the implantation diameters D_-, D_N and D_+, respectively. Table 2 presents the values of RF_-, RF_N and RF_+ for all samples. The *RF* varied within the following ranges: $RF_- \in$ [61.9 N, 93.8 N], $RF_N \in$ [52.7 N, 82.2 N] and $RF_+ \in$ [43.5 N, 66.1 N].

3.3. Multivariate regression analysis

3.3.1. Material parameters vs. heat treatment parameters

Table 3 reports the results from the multivariate linear regression analysis between the heat treatment parameters (T and t; independent

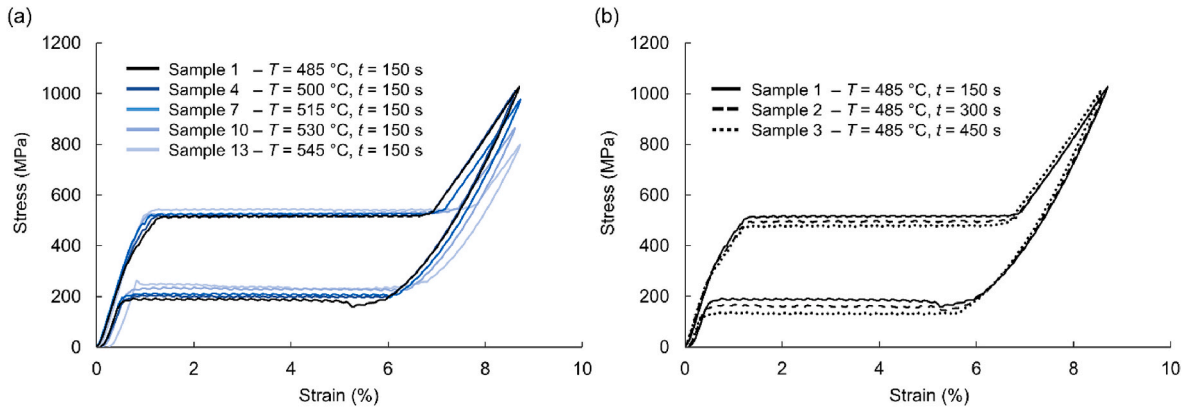

Fig. 5. Uniaxial tensile stress *vs.* strain curve of (a) five NiTi wire samples varying temperature (*T*) and fixing time (*t*); (b) three NiTi wire samples varying *t* and fixing *T*. Only cycle 2 is shown for all NiTi wire samples.

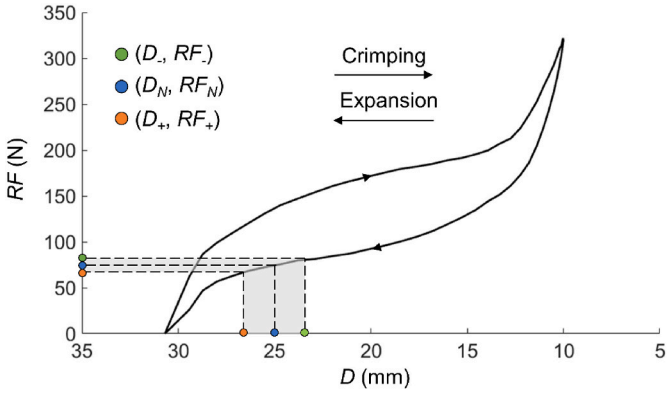

Fig. 6. Radial force (*RF*) *vs.* diameter (*D*) curve obtained from the FE analyses of radial crimping test of the stent-graft, incorporating the material parameters of NiTi wire sample 1. The values of RF_-, RF_N and RF_+, corresponding to D_-, D_N and D_+, respectively, are represented.

variables) and the material parameters (A_f, E_a, E_m, *UPS*, *LPS*, ε_t, ε_r; dependent variables). The results of multivariate linear regression analysis without removal of non-significant parameters and including the root mean squared errors (RMSE) of the measured material parameters are reported in Table S1 of the Supplementary material. Notably, A_f and ε_t exhibited a strong linear dependence only with *T* ($R^2 > 0.92$). E_m, *UPS* and *LPS* exhibited a strong linear relationship with both *T* and *t* ($R^2 > 0.79$). Conversely, E_a exhibited a weak linear dependence on *T* ($R^2 = 0.48$), whereas ε_r exhibited a weak linear dependence on both *T* and *t* ($R^2 = 0.52$). Fig. 7 displays multivariate linear regression models of material parameters with $R^2 > 0.9$, namely A_f, *UPS*, *LPS* and ε_t, with coefficients reported in Table 3. It emerged an inverse relationship between A_f and *T*, and a direct relationship between ε_t and *T*. Additionally, both *UPS* and *LPS* exhibited a direct relationship with *T* and an inverse relationship with *t*.

Table 2
Results of the FE analyses of radial crimping test of the stent-graft incorporating the material parameters of the fifteen NiTi wire samples.

NiTi wire sample	*T* (°C)	*t* (s)	RF_- (N)	RF_N (N)	RF_+ (N)
1	485	150	79.9	68.2	56.9
2	485	300	76.0	66.1	53.4
3	485	450	68.0	55.7	43.5
4	500	150	80.1	68.1	55.5
5	500	300	76.3	66.1	54.1
6	500	450	61.9	52.7	44.3
7	515	150	83.2	72.3	61.3
8	515	300	74.0	65.1	54.7
9	515	450	76.4	66.4	54.2
10	530	150	92.7	80.9	64.3
11	530	300	79.2	69.0	56.3
12	530	450	73.1	63.9	53.6
13	545	150	93.8	82.2	66.1
14	545	300	89.3	78.4	62.5
15	545	450	84.2	74.1	63.6
Minimum	485	150	61.9	52.7	43.5
Maximum	545	450	93.8	82.2	66.1

T: temperature; *t*: time; RF_-, RF_N, RF_+: radial force measured at the implantation diameters D_-, D_N, D_+, respectively.

3.3.2. Stent-graft radial force vs. heat treatment parameters

Table 4 reports the results of the multivariate linear regression analysis between the heat treatment parameters (*T* and *t*; independent variables) and the *RF* quantities (RF_-, RF_N and RF_+; dependent variables). RF_-, RF_N and RF_+ exhibited a strong linear dependence on *T* and *t* ($R^2 > 0.82$). In particular, a direct relationship emerged between RF_-, RF_N, RF_+ and *T* and an inverse relationship between RF_-, RF_N, RF_+ and *t* (Fig. 8). The coefficients of the multivariate linear regression models are reported in Table 4.

3.3.3. Stent-graft radial force vs. material parameters

Table 5 presents the results of the multivariate linear regression analysis between the material parameters (E_a, E_m, *UPS*, *LPS* and ε_t; independent variables) and the *RF* quantities (RF_-, RF_N and RF_+; dependent variables). The results of multivariate linear regression analysis without removal of non-significant parameters are reported in Tables S2 and S3 of the Supplementary material. RF_-, RF_N and RF_+ exhibited a strong direct linear dependence on *LPS* ($R^2 > 0.93$). Conversely, no significant relationship emerged between *RF* quantities and the other NiTi material parameters (Tables S2 and S3 of the Supplementary material). Fig. 9 displays the linear regression models of the *RF* values, with coefficients reported in Table 5.

4. Discussion

The design of NiTi vascular stents encompasses various aspects, including geometry, material, and manufacturing process (Kapoor et al., 2023; Pan et al., 2021). Given the unique characteristics of NiTi, the manufacturing process can substantially impact the mechanical behavior of such devices (Hodgson and Russell, 2000; Liu and Mishnaevsky, 2013; Mwangi et al., 2019; Valiev et al., 2020). Heat treatment is a key process for the manufacturing of NiTi vascular stents. While commonly used for the shape-setting of the device, heat treatment can also have a remarkable impact on the mechanical properties of the material and, consequently, on the mechanical behavior of the NiTi

Table 3
Results of the multivariate linear regression analysis between the heat treatment parameters and the material parameters after removal of non-significant parameters.

Material parameter	R^2	F-test *p*-value	T *p*-value	t *p*-value	c_0	c_T	c_t
A_f (°C)	0.96	<0.001	<0.001	–	2.33E+02 °C	−4.28E-01	–
E_a (MPa)	0.48	0.004	0.004	–	4.32E+04 MPa	3.38E+01 MPa/°C	–
E_m (MPa)	0.79	<0.001	<0.001	0.003	4.26E+04 MPa	−2.93E+01 MPa/°C	−3.33E+00 MPa/s
UPS (MPa)	0.94	<0.001	<0.001	<0.001	3.45E+02 MPa	3.92E-01 MPa/°C	−1.38E-01 MPa/s
LPS (MPa)	0.92	<0.001	<0.001	<0.001	−2.62E+02 MPa	9.70E-01 MPa/°C	−1.66E-01 MPa/s
ε_t (%)	0.92	<0.001	<0.001	–	−2.66E+00 %	1.53E-02 1/°C	–
ε_r (%)	0.52	0.013	0.025	0.028	−7.67E-01 %	2.29E-031/°C	3.87E-04 1/s

R^2: coefficient of determination; c_0, c_T, c_t: coefficients of the multivariate linear regression models corresponding to the constant term, T and t, respectively; T: temperature; t: time; A_f: austenite finish temperature; E_a: austenite elastic modulus; E_m: martensite elastic modulus; *UPS*: upper plateau stress; *LPS*: lower plateau stress; ε_t: transformation strain; ε_r: residual strain.

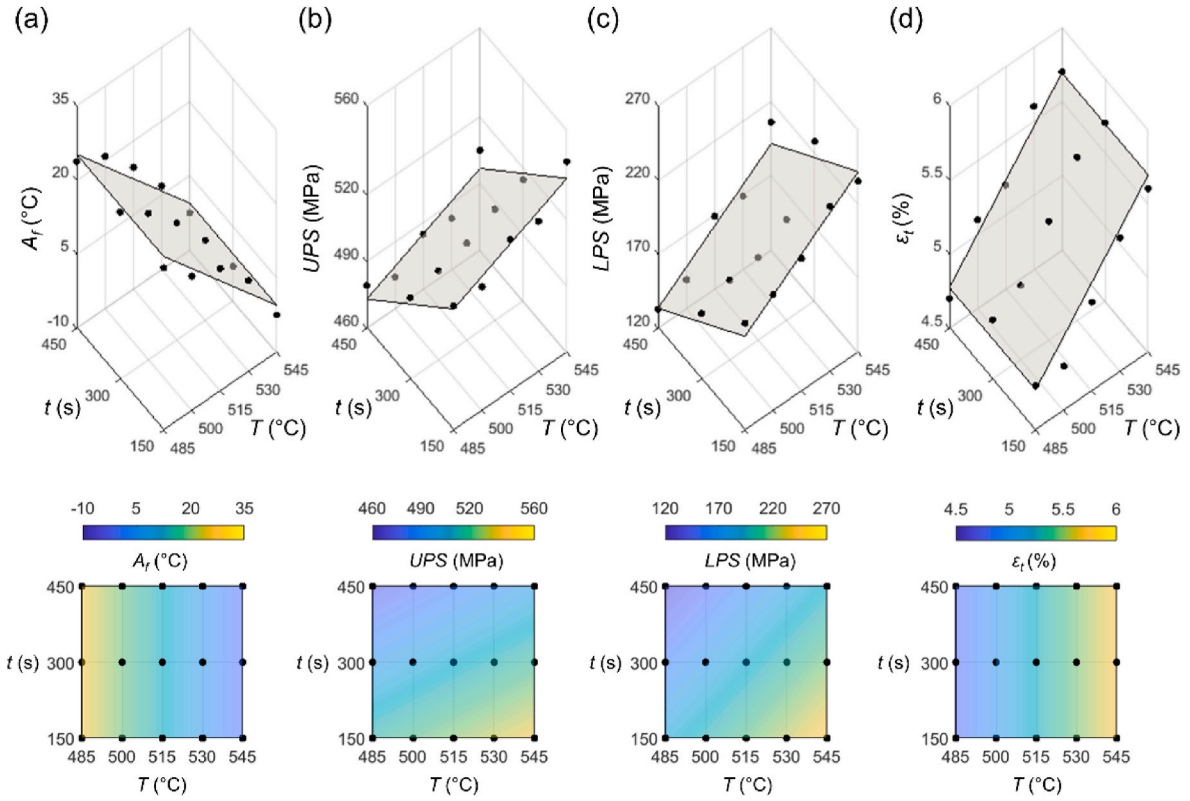

Fig. 7. Multivariate linear regression models of (a) austenite finish temperature (A_f), (b) upper plateau stress (*UPS*), (c) lower plateau stress (*LPS*) and (d) transformation strain (ε_t) as a function of the heat treatment parameters temperature (T) and time (t), represented as transparent grey planes. The values measured in the experimental tests are represented as black dots.

Table 4
Results of the multivariate linear regression analysis between heat treatment parameters and the stent-graft radial force.

RF	R^2	*F-test p-value*	T *p*-value	t *p*-value	c_0	c_T	c_t
RF. (N)	0.82	<0.001	<0.001	<0.001	−3.77E+01 N	2.53E-01 N/°C	−4.40E-02 N/s
RF_N (N)	0.84	<0.001	<0.001	<0.001	−5.27E+01 N	2.58E-01 N/°C	−3.92E-02 N/s
RF_+ (N)	0.84	<0.001	<0.001	<0.001	−4.59E+01 N	2.16E-01 N/°C	−2.99E-02 N/s

R^2: coefficient of determination; c_0, c_T, c_t: coefficients of the multivariate linear regression models corresponding to the constant term, T and t, respectively; T: temperature; t: time; RF_-, RF_N, RF_+: radial force measured at the implantation diameters D_-, D_N, D_+, respectively.

device. This aspect was not adequately addressed in the currently available body of literature. In a very recent study (Bernini et al., 2024) it was proposed to design self-expandable vascular stents with innovative geometries through heat treatment for shape-setting. Accordingly, heat treatment was applied to vascular stents considering various values of T and t, and the *RF* exerted by stents was measured

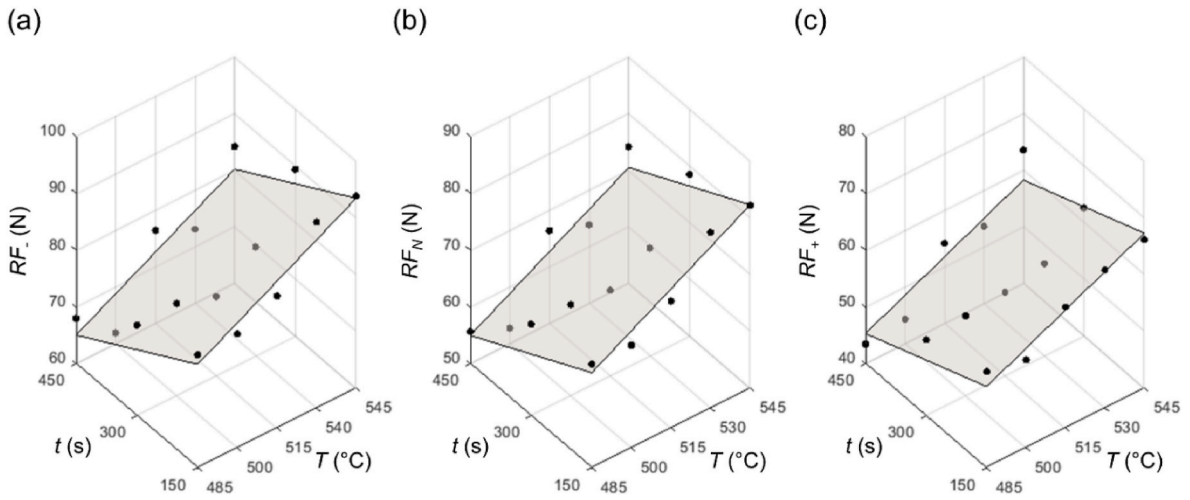

Fig. 8. Multivariate linear regression models of the radial force (*RF*) as a function of heat treatment parameters temperature (*T*) and time (*t*), represented as transparent grey planes. The values of *RF* computed in the FE analyses are represented as black dots. RF_-, RF_N and RF_+ correspond the *RF* measured at the implantation diameters D_-, D_N, D_+, respectively.

Table 5
Results of the multivariate linear regression analysis between the material parameters and stent-graft radial force after removal of non-significant parameters.

RF	R^2	F-test *p*-value	*LPS* *p*-value	c_0	c_{LPS}
RF_- (N)	0.94	<0.001	<0.001	2.86E+01 N	2.70E-01 N/MPa
RF_N (N)	0.94	<0.001	<0.001	2.05E+01 N	2.57E-01 N/MPa
RF_+ (N)	0.93	<0.001	<0.001	1.78E+01 N	2.05E-01 N/MPa

R^2: coefficient of determination; c_0, c_{LPS}: coefficients of the multivariate linear regression models corresponding to the constant term and to *LPS*, respectively; *T*: temperature; *t*: time; *LPS*: lower plateau stress; RF_-, RF_N, RF_+: radial force measured at the implantation diameters D_-, D_N, D_+, respectively.

experimentally to investigate the impact of the heat treatment parameters on the mechanical performance of the designed devices. However, only a limited number of values of *T* and *t* were considered, and the relationship between the heat treatment parameters and the *RF* exerted by the stents was not thoroughly explored. In contrast, in the present study, considering a stent-graft and the radial crimping procedure as an illustrative case, a combined experimental and computational approach complemented by multivariate linear regression analysis was employed to explore the relationships among the heat treatment parameters, the material properties of NiTi, and the mechanical behavior of the stent-graft. The results of the study confirm that the mechanical behavior of the stent-graft can be significantly affected by the parameters of the heat treatment *T* and *t*. Importantly, the findings of the study imply the feasibility of tailoring/improving the mechanical behavior of the device solely through adjustments in heat treatment parameters, without altering the geometry. This offers clear advantages in terms of times and costs associated to the industrial development of the device.

To support the adoption of the heat treatment control to properly tune the design of the NiTi device, this study proposes a rapid and robust design tool based on regression models. This tool enables the design and optimization of the mechanical behavior of a specific NiTi vascular stent (in this case, a stent-graft) under a specific loading condition (in this case, radial load) through adjustment of the heat treatment parameters. Additionally, this tool can complement computational frameworks that enable the optimization of the mechanical response of the device by acting on the geometry, the use of which has been widely demonstrated in the literature (Alaimo et al., 2017; Barati et al., 2022; Carbonaro et al., 2021, 2023c; Kapoor et al., 2023; Liu et al., 2023). The main relationships identified in the present study are discussed in the following subsections and summarized in Fig. 10.

4.1. Material parameters vs. heat treatment parameters

Applying heat treatment to NiTi leads to the dispersion of nickel-rich

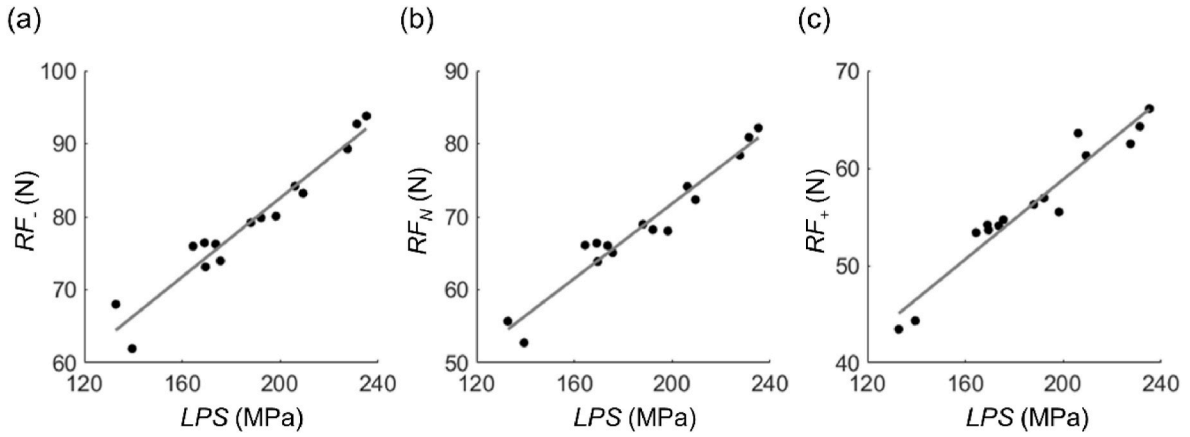

Fig. 9. Linear regression models of the radial force (*RF*) as a function of lower plateau stress (*LPS*), represented as grey lines. The values of *RF* computed in the FE analyses are represented as black dots. RF_-, RF_N and RF_+ correspond the *RF* measured at the implantation diameters D_-, D_N, D_+, respectively.

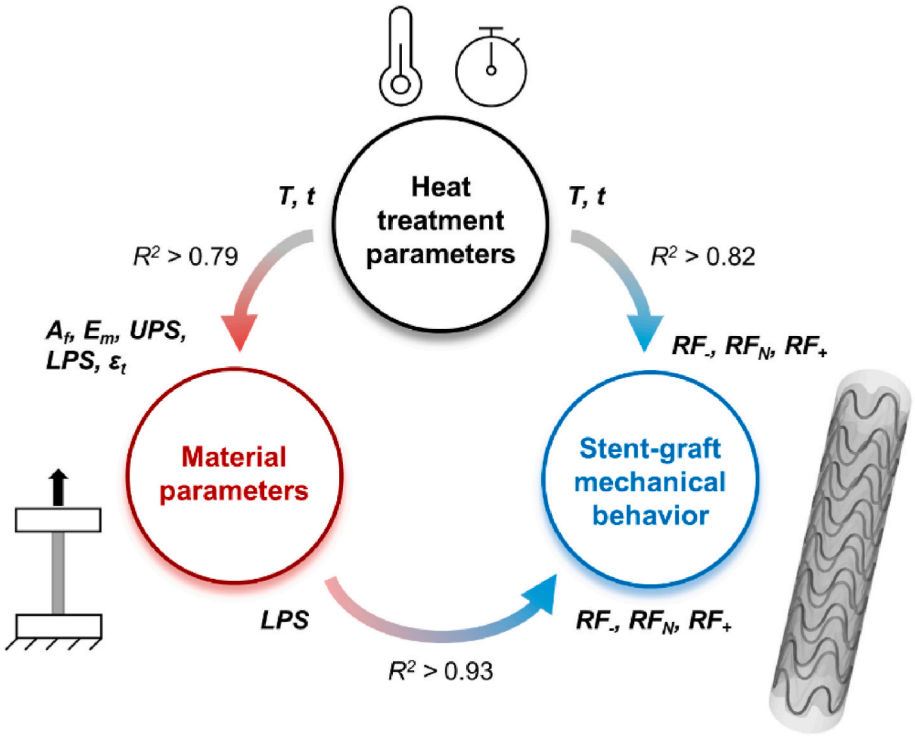

Fig. 10. Main relationships investigated in this study: (i) between the heat treatment parameters and the material parameters of NiTi, (ii) between the heat treatment parameters and the mechanical behavior of the stent-graft, and (iii) between the material parameters of NiTi and the mechanical behavior of the stent-graft.

precipitates and to dislocations in the matrix (Aboutalebi et al., 2015; Agarwal et al., 2023), thereby altering the material characteristics. The results of this study underscore the significant impact of the heat treatment procedure on the super-elastic properties of NiTi material. Specifically, it was observed that certain super-elastic material parameters (i.e., A_f, E_m, *UPS*, *LPS* and ε_t) exhibit a strong linear dependence with the heat treatment parameters, within the explored range of T and t. Accordingly, the implemented regression models allow for the a priori determination of A_f, E_m, *UPS*, *LPS* and ε_t through adjustments of T and t.

When comparing the findings of this study with those of previous experimental investigations, it is important to consider that the results are dependent on the specific chemical composition of the NiTi alloy and on the specific range of T and t considered for the heat treatment. Previous studies reported that increasing values of T (varying in a range comparable to the one analyzed in the present study) lead to decreasing values of A_f (Agarwal et al., 2023; Bernini et al., 2024; Liu et al., 2008; Zhan et al., 2020), a finding consistent with the results of this study. In contrast to the present study, which did not reveal a significant relationship between A_f and t, previous studies (Agarwal et al., 2023; Bernini et al., 2024; Liu et al., 2008; Zhan et al., 2020) reported that increasing values of t result in increasing values of A_f. Nevertheless, these studies examined time intervals of application of heat treatment up to 180 min, which are much longer than those analyzed here (150 s – 450 s). Finally, in accordance with the present study, Liu et al. (2008) reported that when accounting for T and t values comparable to those analyzed here, increasing T and t resulted in increasing and decreasing values of both *UPS* and *LPS*, respectively.

4.2. Stent-graft radial force vs. heat treatment parameters

Variations in the super-elastic properties of NiTi, associated with various heat treatment parameters, result in a different mechanical behavior of NiTi vascular stents (Carbonaro et al., 2023d). This study confirms this effect, demonstrating a substantial variation in the *RF* generated by the stent-graft when varying the heat treatment parameters T and t. Specifically, RF_-, RF_N and RF_+ increased by 52 %, 56 % and 52 %, respectively, compared to their minimum values. Moreover, the *RF* values exhibited a strong linear dependence on the heat treatment parameters within the explored range of T and t. In this regard, the implemented regression models enable design and optimization of the mechanical behavior of the stent-graft solely by adjusting the heat treatment parameters, achieving considerable variations in the *RF* generated by the stent-graft during implantation.

Interestingly, the findings of this study can be qualitatively compared with those of Bernini et al. (2024), where the effect of different heat treatments parameters on the mechanical characteristics of laser-cut and wire-braided NiTi stents was investigated. Consistent with the present study, it was reported that *RF* values, measured in the expansion step of the radial crimping procedure, increase as T increases and as t decreases, independent of the fabrication approach.

4.3. Stent-graft radial force vs. material parameters

Results highlight a strong linear dependence of the radial force from *LPS*, with increasing *RF* values as *LPS* increases within the investigated range of T and t. On the contrary, no association of *RF* with the other material parameters (i.e., E_a, E_m, *UPS* and ε_t) emerged. This result can be attributed to the fact that the hysteresis of the *RF vs. D* curve is linked to the super-elastic stress *vs.* strain curve (see Fig. 1, steps 2 and 3) (Stoeckel et al., 2004). More specifically, the crimping procedure is a displacement-controlled procedure in which the stent-graft is loaded (crimping step) and unloaded (expansion step). As a result, the stress and strain values of the stent-graft increase during the crimping step and decrease during the expansion step, transitioning into the lower plateau, which is identified by the *LPS*. In this context, higher values of *LPS* results in higher stress values of the stent-graft and, consequently, in higher *RF* values at the implantation diameters. It is also expected that only the material parameters related to the stress *vs.* strain unloading curve (i.e., E_a and *LPS*) have a substantial impact on the *RF* values. However, here no significant relationship was observed between the *RF*

values and E_a, because of the small variation of E_a (5 %, compared to the minimum value) observed by varying the heat treatment parameters. These findings qualitatively agree with those of a previous computational study (Carbonaro et al., 2023d), which investigated the impact of the super-elastic material properties of NiTi on the mechanical performance of the NiTi frame of transcatheter aortic valves. In particular, the study observed that the stress values identifying the *LPS* had the greatest impact on the *RF* generated by the device at implantation, compared to the other super-elastic material parameters. Additionally, it was observed that increasing values of the *LPS* lead to increasing *RF* values at the implantation diameters.

4.4. Limitations and future perspectives

The exact chemical composition and the microscopic characteristics of the NiTi wire were not provided by the material supplier. No experimental investigation for their assessment was conducted to assess these aspects as it was beyond the scope the study. The effect of heat treatment on the mechanical properties of NiTi was analyzed through the implementation of multivariate regression models, without investigating the microstructure changes within the material. A single NiTi wire sample per heat treatment was tested and, consequently, it was not feasible to assess the uncertainty associated with the replication of each testing condition. However, given the experimental design of the fifteen NiTi wire samples, the uncertainty of the experimental results was evaluated in the multivariate regression analysis in terms of RMSE. Moreover, experimental tests were conducted on NiTi wire samples, considering a single production lot and a sole supplier of NiTi, within a restricted range of heat treatment parameters T and t. To broaden the scope of the research, specimens with diverse chemical compositions, obtained from different production lots and suppliers, could be included. The impact of heat treatment was solely assessed concerning the super-elastic properties of the NiTi material, and its effects on fatigue characteristics and biocompatibility was not evaluated. Moreover, this study exclusively investigated the impact of heat treatment on the mechanical response of a stent-graft under radial loading conditions. However, NiTi vascular stents can undergo a plethora of loading conditions during insertion and after implantation, including axial, bending and torsion loads, as well as complex loading states. Additional mechanical tests (ISO, 2012) could be performed *in silico* following the procedure presented here for the crimping test. Furthermore, the effect of heat treatment may depend on the geometry of the NiTi samples or stents to which it is applied. While wire samples and stent-grafts were the focus of this study, future investigations could encompass samples with different dimensions and other types of NiTi vascular stents, whose structure is not composed of NiTi wires but is instead obtained through laser cutting from a NiTi cylinder.

5. Conclusions

The present study highlights the potential to design and optimize the mechanical response of NiTi vascular stents by tuning the heat treatment parameters T and t. In particular, the results demonstrate a significant impact of heat treatment parameters on both the super-elastic properties of NiTi and on the mechanical behavior of a NiTi stent-graft under radial loading conditions. These findings suggest the feasibility of enhancing the mechanical behavior of NiTi stent-grafts, and more in general of NiTi vascular stents, without altering the geometry but solely by properly tuning the heat treatment parameters. Accordingly, the here identified regression models linking the heat treatment parameters with both the NiTi material properties and the radial force exerted by the stent-graft, can be used as functional tool for tuning T and t to achieve the desired NiTi material properties and mechanical characteristics of the device. Finally, the approach proposed in this study offers adequate flexibility to be extended to other implantable NiTi cardiovascular devices.

CRediT authorship contribution statement

Dario Carbonaro: Writing – review & editing, Writing – original draft, Visualization, Software, Methodology, Investigation, Formal analysis, Data curation, Conceptualization. **Elena Villa:** Writing – review & editing, Resources, Investigation, Data curation. **Diego Gallo:** Writing – review & editing, Formal analysis. **Umberto Morbiducci:** Writing – review & editing, Supervision. **Alberto Luigi Audenino:** Writing – review & editing, Supervision, Funding acquisition, Conceptualization. **Claudio Chiastra:** Writing – review & editing, Writing – original draft, Supervision, Project administration, Methodology, Conceptualization.

Declaration of competing interest

The authors declare that they have no known competing financial interests or personal relationships that could have appeared to influence the work reported in this paper.

Data availability

Data will be made available on request.

Acknowledgements

The authors express their gratitude to Francesco Bonetti and Franco Osta (AorticLab srl, Italy) for their support. Additionally, the authors have received financial support from the Piedmont Region, Italy (POR FESR PiTeF 2014-20 351-96, Nitiliera).

Appendix A. Supplementary data

Supplementary data to this article can be found online at https://doi.org/10.1016/j.jmbbm.2024.106653.

References

Aboutalebi, M.R., Karimzadeh, M., Salehi, M.T., Abbasi, S.M., Morakabati, M., 2015. Influences of aging and thermomechanical treatments on the martensitic transformation and superelasticity of highly Ni-rich Ti-51.5 at.% Ni shape memory alloy. Thermochim. Acta 616, 14–19. https://doi.org/10.1016/j.tca.2015.08.004.

Agarwal, N., Ryan Murphy, J., Hashemi, T.S., Mossop, T., O'Neill, D., Power, J., Shayegh, A., Brabazon, D., 2023. Effect of heat treatment time and temperature on the microstructure and shape memory properties of Nitinol wires. Materials 16, 6480. https://doi.org/10.3390/ma16196480.

Alaimo, G., Auricchio, F., Conti, M., Zingales, M., 2017. Multi-objective optimization of Nitinol stent design. Med. Eng. Phys. 47, 13–24. https://doi.org/10.1016/j.medengphy.2017.06.026.

ASTM, 2018. F2063 - Wrought Nickel-Titanium Shape Memory Alloys for Medical Devices and Surgical Implants.

ASTM, 2015. F2005 - Standard Terminology for Nickel-Titanium Shape Memory Alloys.

Auricchio, F., Taylor, R.L., 1997. Shape-memory alloys: modelling and numerical simulations of the finite-strain superelastic behavior. Comput. Methods Appl. Mech. Eng. 143, 175–194. https://doi.org/10.1016/S0045-7825(96)01147-4.

Auricchio, F., Taylor, R.L., Lubliner, J., 1997. Shape-memory alloys: Macromodelling and numerical simulations of the superelastic behavior. Comput. Methods Appl. Mech. Eng. 146, 281–312. https://doi.org/10.1016/S0045-7825(96)01232-7.

Barati, S., Fatouraee, N., Nabaei, M., Petrini, L., Migliavacca, F., Luraghi, G., Felix, J., Matas, R., 2022. Patient-specific multi-scale design optimization of transcatheter aortic valve stents. Comput. Methods Progr. Biomed. 221, 106912 https://doi.org/10.1016/j.cmpb.2022.106912.

Bernini, M., Hellmuth, R., Sullivan, M.O., Dunlop, C., Mckenna, C.G., Lucchetti, A., Gries, T., Ronan, W., Vaughan, T.J., 2024. Shape-setting of self-expanding nickel–titanium laser-cut and wire-braided stents to introduce a helical ridge. Cardiovasc. Eng. Technol. https://doi.org/10.1007/s13239-024-00717-2.

Cabrera, M.S., Oomens, C.W.J., Baaijens, F.P.T., 2017. Understanding the requirements of self-expandable stents for heart valve replacement: radial force, hoop force and equilibrium. J. Mech. Behav. Biomed. Mater. 68, 252–264. https://doi.org/10.1016/j.jmbbm.2017.02.006.

Carbonaro, D., Chiastra, C., Bologna, F.A., Audenino, A.L., Terzini, M., 2024. Determining the mechanical properties of super-elastic nitinol bone staples through an integrated experimental and computational calibration approach. Ann. Biomed. Eng. 52, 682–694. https://doi.org/10.1007/s10439-023-03416-6.

Carbonaro, D., Chiastra, C., Morbiducci, U., Audenino, A., 2020. Transcatheter aortic valve with embolic filter: experiments and simulations. In: Proceedings of VII

Congress of the National Group of Bioengineering. https://www.scopus.com/record/display.uri?eid=2-s2.0-85149381560&origin=resultslist.
Carbonaro, D., Gallo, D., Morbiducci, U., Audenino, A., Chiastra, C., 2021. In silico biomechanical design of the metal frame of transcatheter aortic valves: multi-objective shape and cross-sectional size optimization. Struct. Multidiscip. Optim. 64, 825–1842. https://doi.org/10.1007/s00158-021-02944-w.
Carbonaro, D., Lucchetti, A., Audenino, A.L., Gries, T., Vaughan, T.J., Chiastra, C., 2023b. Multi-objective design optimization of bioresorbable braided stents. Comput. Methods Progr. Biomed. 242, 107781 https://doi.org/10.1016/j.cmpb.2023.107781.
Carbonaro, D., Mezzadri, F., Ferro, N., De Nisco, G., Luigi, A., Gallo, D., Chiastra, C., Morbiducci, U., Perotto, S., 2023c. Design of innovative self-expandable femoral stents using inverse homogenization topology optimization. Comput. Methods Appl. Mech. Eng. 416, 116288 https://doi.org/10.1016/j.cma.2023.116288.
Carbonaro, D., Zambon, S., Corti, A., Gallo, D., Morbiducci, U., Audenino, L., Chiastra, C., 2023d. Impact of nickel – titanium super-elastic material properties on the mechanical performance of self-expandable transcatheter aortic valves. J. Mech. Behav. Biomed. Mater. 138, 105623 https://doi.org/10.1016/j.jmbbm.2022.105623.
Catanese, J., Cooke, D., Maas, C., Pruitt, L., 1999. Mechanical properties of medical grade expanded polytetrafluoroethylene: the effects of internodal distance, density, and displacement rate. J. Biomed. Mater. Res. 48, 187–192. https://doi.org/10.1002/(SICI)1097-4636(1999)48:2<187::AID-JBM13>3.0.CO;2-M.
Duerig, T., Melton, K.N., Stoeckel, D., 1990. Engineering aspects of shape memory alloys. Engineering Aspects of Shape Memory Alloys. Elsevier. https://doi.org/10.1016/c2013-0-04566-5.
Duerig, T., Stoeckel, D., Johnson, D., 2003. Smart materials for medical applications. In: European Workshop on Smart Structures in Engineering and Technology.
Fanning, J.P., Platts, D.G., Walters, D.L., Fraser, J.F., 2013. Transcatheter aortic valve implantation (TAVI): valve design and evolution. Int. J. Cardiol. 168, 1822–1831. https://doi.org/10.1016/j.ijcard.2013.07.117.
FDA, 2010. Non-clinical Engineering Tests and Recommended Labeling for Intravascular Stents and Associated Delivery Systems.
Freund, R.J., Wilson, W.J., Mohr, D.L., 2010. Chapter 7 - linear regression. In: Freund, R. J., Wilson, W.J., Mohr, D.L. (Eds.), Statistical Methods, third ed. Academic Press, Boston, pp. 321–374. https://doi.org/10.1016/B978-0-12-374970-3.00007-X.
Henderson, E., Nash, D.H., Dempster, W.M., 2011. On the experimental testing of fine Nitinol wires for medical devices. J. Mech. Behav. Biomed. Mater. 4, 261–268. https://doi.org/10.1016/j.jmbbm.2010.10.004.
Hodgson, D., Russell, S., 2000. Nitinol melting, manufacture and fabrication. Minim Invasive Ther. Allied Technol. 9, 61–65. https://doi.org/10.3109/13645700009063051.
ISO, 2012. Cardiovascular Implants — Endovascular Devices — Part 2: Vascular Stents.
Kan, X., Ma, T., Lin, J., Wang, L., Dong, Z., Xu, X.Y., 2021. Patient-specific simulation of stent-graft deployment in type B aortic dissection: model development and validation. Biomech. Model. Mechanobiol. 20, 2247–2258. https://doi.org/10.1007/s10237-021-01504-x.
Kapoor, A., Jepson, N., Bressloff, N.W., Loh, P.H., Ray, T., Beier, S., 2023. The road to the ideal stent: a review of stent design optimisation methods, findings, and opportunities. Mater. Des. 237, 112556 https://doi.org/10.1016/j.matdes.2023.112556.
Kapoor, D., 2017. Nitinol for medical applications: a brief introduction to the properties and processing of nickel titanium shape memory alloys and their use in stents. Johnson Matthey Technol. Rev. 61, 66–76. https://doi.org/10.1595/205651317X694524.
Kleinstreuer, C., Li, Z., Basciano, C.A., Seelecke, S., Farber, M.A., 2008. Computational mechanics of Nitinol stent grafts. J. Biomech. 41, 2370–2378. https://doi.org/10.1016/j.jbiomech.2008.05.032.
Liu, H.S., Mishnaevsky, L., 2013. Martensitic transformations in nanostructured nitinol: finite element modeling of grain size and distribution effects. Comput. Mater. Sci. 76, 27–36. https://doi.org/10.1016/j.commatsci.2012.11.032.
Liu, X., Wang, Y., Yang, D., Qi, M., 2008. The effect of ageing treatment on shape-setting and superelasticity of a Nitinol stent. Mater. Char. 59, 402–406. https://doi.org/10.1016/j.matchar.2007.02.007.
Liu, Z., Chen, G., Ong, C., Yao, Z., Li, X., Deng, J., Cui, F., 2023. Multi-objective design optimization of stent-grafts for the aortic arch. Mater. Des. 227, 111748 https://doi.org/10.1016/j.matdes.2023.111748.
Mwangi, J.W., Nguyen, L.T., Bui, V.D., Berger, T., Zeidler, H., Schubert, A., 2019. Nitinol manufacturing and micromachining: a review of processes and their suitability in processing medical-grade Nitinol. J. Manuf. Process. 38, 355–369. https://doi.org/10.1016/j.jmapro.2019.01.003.
Otsuka, K., Ren, X., 2005. Physical metallurgy of Ti-Ni-based shape memory alloys. Prog. Mater. Sci. 50, 511–678. https://doi.org/10.1016/j.pmatsci.2004.10.001.
Pan, C., Han, Y., Lu, J., 2021. Structural design of vascular stents: a review. Micromachines 12, 1–26. https://doi.org/10.3390/mi12070770.
Pelton, A.R., DiCello, J., Miyazaki, S., 2000. Optimisation of processing and properties of medical grade Nitinol wire. Minim Invasive Ther. Allied Technol. 9, 107–118. https://doi.org/10.3109/13645700009063057.
Ramella, A., Migliavacca, F., Rodriguez Matas, J.F., Heim, F., Dedola, F., Marconi, S., Conti, M., Allievi, S., Mandigers, T.J., Bissacco, D., Domanin, M., Trimarchi, S., Luraghi, G., 2022. Validation and verification of high-fidelity simulations of thoracic stent-graft implantation. Ann. Biomed. Eng. 50, 1941–1953. https://doi.org/10.1007/s10439-022-03014-y.
Senf, B., von Sachsen, S., Neugebauer, R., Drossel, W.G., Florek, H.J., Mohr, F.W., Etz, C. D., 2014. The effect of stent graft oversizing on radial forces considering Nitinol wire behavior and vessel characteristics. Med. Eng. Phys. 36, 1480–1486. https://doi.org/10.1016/j.medengphy.2014.07.020.
Stoeckel, D., Pelton, A., Duerig, T., 2004. Self-expanding Nitinol stents: material and design considerations. Eur. Radiol. 14, 292–301. https://doi.org/10.1007/s00330-003-2022-5.
Valiev, R.Z., Prokofiev, E.A., Kazarinov, N.A., Raab, G.I., Minasov, T.B., Stráský, J., 2020. Developing nanostructured Ti alloys for innovative implantable medical devices. Materials 13, 967. https://doi.org/10.3390/ma13040967.
Zarins, C.K., Bloch, D.A., Crabtree, T., Matsumoto, A.H., White, R.A., Fogarty, T.J., May, J., 2003. Stent graft migration after endovascular aneurysm repair: importance of proximal fixation. J. Vasc. Surg. 38, 1264–1272. https://doi.org/10.1016/S0741-5214(03)00946-7.
Zhan, Y., He, L., Lu, X., Zhu, X., Chen, Q., 2020. The effect of ageing treatment on shape-setting and shape memory effect of a NiTi SMA corrugated structure. Adv. Mater. Sci. Eng. 2020 https://doi.org/10.1155/2020/2846721.